Materials Advances

ROYAL SOCIETY OF CHEMISTRY

PAPER

View Article Online
View Journal

Cite this: DOI: 10.1039/d6ma00022c

pH-Responsive carborhodol-coupled chitosan-based hydrogels for the detection of wound infection-relevant pH changes

Aswathi Syam, †[a] Nicola Cusick, †[b] Alexander Zilles [a] and Holger Schönherr *[b]

Wound infections are typically accompanied by an elevated local pH, resulting from bacterial metabolism. Smart wound dressings capable of sensing and reporting these pH changes could enable clinicians to detect infections at an early stage and begin appropriate treatment. However, conventional pH-responsive dyes often lack photostability and exhibit subtle or ambiguous color changes. In this work, we report the synthesis of two novel carborhodol dyes, AS 14 and AS 15, which exhibit reversible chromogenic and fluorogenic responses within the physiologically relevant pH range of 4–7. The NHS-esters of these dyes were covalently coupled to chitosan (CS) films, yielding stable, biopolymer-based sensors. Both AS 14-CS and AS 15-CS films demonstrated high photostability, reversible pH-dependent responses, and distinct fluorescence lifetime changes. Notably, AS 14-CS exhibited dual chromogenic and fluorogenic responses, achieving a fluorescence turn-on ratio of 30 in basic *versus* acidic form, while AS 15-CS functioned primarily as a chromogenic sensor, exhibiting a color change from pink to blue. By covalently coupling the novel carborhodols, the pH response is stable over time. The possibility of relying on fluorescence lifetime measurements also enables measurement in autofluorescent wound environments, which is not possible for dyes with shorter lifetimes. These pH-responsive films offer a robust and sensitive platform for further development into infection-responsive wound dressings, with AS 14-CS in particular providing dual-mode sensing in one film, enabling both naked-eye visualization and higher-sensitivity fluorescent readouts without requiring any on-patch electronics.

Received 5th January 2026,
Accepted 30th March 2026

DOI: 10.1039/d6ma00022c

rsc.li/materials-advances

Introduction

Around 20 million people worldwide are currently affected by a chronic, or non-healing, wound.[1] Colonization of wounds by microorganisms is common, making wound infections the most prevalent type of hospital-acquired infection across the globe.[2] Clinicians typically identify infection *via* visual observations.[3,4] However, in patients with chronic wounds, infection detection often relies on subtle signs of infection, such as odor or delayed healing.[3,5] Misdiagnosis can lead to prolonged hospitalization and systemic infection.[6] There is therefore a need for new methods to alert clinicians to the presence of an infection. While advanced imaging techniques such as computed tomography and magnetic resonance imaging can be utilized, their high cost and limited accessibility make them impractical for routine use.[6] In contrast, point-of-care, wearable biosensors have emerged as a promising tool for real-time monitoring of wound status, a trend further driven by the rapidly expanding wound care market, projected to reach US$31 billion by the end of 2030.[7]

The concept of detecting biomarkers present in infected wound sites has been used to develop a variety of sensors.[8] Enzymes or toxins secreted by bacteria can be used as stimuli in smart materials, for example, hyaluronidase-sensitive polymersomes,[9] toxin-sensitive liposomes,[10] pyocyanin-sensitive carbon ultramicroelectrode arrays,[11] protease-sensitive nanoporous silicon rugate filters,[12] and β-glucuronidase-sensitive chitosan films.[13] However, these markers are often disease- or stage-specific, or the sensor requires external input.[14] In contrast, wound pH has been suggested as a more general diagnostic marker of wound infection, providing good sensitivity to the presence of infection while remaining simple to interpret.[15] Healthy skin surfaces exhibit an acidic milieu with a pH of 4.1–5.8, while the pH of infected wounds is elevated by the alkaline byproducts of bacterial proliferation, including ammonia from

[a] *ATTO-TEC GmbH, Martinshardt 7, 57074 Siegen, Germany*
[b] *Physical Chemistry I & Research Center of Micro- and Nanochemistry and (Bio)Technology (Cμ), Department of Chemistry and Biology, School of Science and Technology, University of Siegen, 57076 Siegen, Germany.*
E-mail: schoenherr@chemie.uni-siegen.de
† These authors contributed equally.

amino acid metabolism, and can be characterized by a pH above 7.3.[16,17] Moreover, the presence of necrotic tissue in the wound bed increases the metabolic load, often leading to tissue hypoxia and sustained inflammation.[18] This environment is typically characterized by elevated levels of inflammatory exudate and proteolytic enzymes. Although precise prediction of wound pH based on infection status is debated in the literature, detection of elevated pH levels could provide an indication for the requirement for intervention.[19]

Biosensors capable of detecting this pH elevation provide a simple, non-invasive method for early detection of infection. Optical biosensors, which detect an analyte and result in a shift in light absorbance or emission, have been developed to monitor temperature, pH, and oxygen.[7] However, many rely on advanced technologies and transducers, raising costs and limiting translation to the clinic.[7,20] An alternative strategy for providing a simple indication of pH without the need for complex electrochemical systems is the incorporation of pH-sensitive dyes into a carrier material, which reports pH changes through visible readouts.[21,22] By combining a pH-sensitive dye with a hydrogel, a simple, low-cost wound dressing sensitive to the presence of infection is possible.

Hydrogels are widely used in wound care as a dressing material due to their biocompatibility, biodegradability, and ability to maintain a moist healing environment.[23] Chitosan, a cationic polysaccharide obtained *via* deacetylation of chitin, is a particularly attractive wound dressing material.[24] Composed of glucosamine and *N*-acetyl glucosamine units, chitosan acts as a natural template, emulating the extracellular matrix and promoting tissue regeneration.[7] Chitosan is also antifouling, minimizing protein adsorption and cell adhesion, which is necessary to maintain the performance of a wearable sensor.[7,25] Its free hydroxyl and amino groups enable chemical modification, which has been exploited for conjugation of dyes, polymers, and bioactive molecules.[13,26–28] Covalent attachment of pH-sensitive dye molecules has emerged as a promising approach for modifying chitosan, as the dye cannot leach from the films.[24] Previous studies have reported chitosan chemically grafted with phenol red, rosolic acid, methyl red and rose Bengal to yield colorimetric pH-sensors.[29,30] However, these dyes typically exhibit low photostability, and detection of pH changes relies on shifts in the absorption, rather than more sensitive fluorescence-based changes.[31,32] In addition, many azo dyes, including methyl red, are toxic, raising concerns for clinical use.[33]

Alternative strategies, such as hybrid hydrogels containing silver nanoparticles functionalized with red cabbage extract, have been explored, but their color changes from red to green at pH 7–8 can be confounded by the natural appearance of the wound bed.[34] Similarly, limited contrast has also been demonstrated with phenol red-based sensors.[35,36] For practical wound diagnostics, an ideal system should exhibit a high-contrast optical shift, preferably spanning distinct regions of the visible spectrum. For example, a red-to-blue transition is readily perceptible, minimally affected by color vision deficiencies, and therefore less likely to be misinterpreted. In addition, since dressings are often applied for several days, the sensing dye must be highly photostable to ensure reliable long-term monitoring. Fluorescein-based dyes, although widely used, are unsuitable due to rapid photobleaching, leading to loss of fluorescence intensity and, therefore, loss of sensitivity over time.[37] The development of more photostable pH-sensitive dyes is essential for clinical translation of smart wound dressings.

This study therefore aims to combine the advantages of covalent immobilization of a fluorophore to CS, providing a stable readout, with a novel pH-sensitive dye capable of providing both a visible color change and a fluorescence enhancement upon pH changes. This work is based on carborhodols, a distinct subclass of rhodol derivatives first reported by Sednev *et al.* in 2013, where they were employed for two-color fluorescence imaging.[38] An alternative synthetic route to the carborhodol scaffold was described by Jia *et al.* in 2018, extending its utility by preparing copper-sensitive probes.[39] Despite these studies, carborhodols have received relatively limited attention, and their potential as pH-responsive probes remains largely unexplored. ATTO-TEC has reported that carborhodol dyes display photostability along with pH-dependent chromogenic and fluorogenic behavior (patent filed).[40]

In this work, two novel, photostable, pH-responsive carborhodol derivatives, AS 14 and AS 15, are coupled to chitosan hydrogels using DCC/NHS chemistry. These dye-coupled hydrogels are characterized by attenuated total internal reflection Fourier transform infrared (ATR FTIR) spectroscopy and field-emission scanning electron microscopy (FESEM). Their swelling behavior, photostability, and pH-responsive behavior are investigated. These films function as both chromogenic and fluorogenic sensors with excellent color stability and no dye leaching. In combination with a mechanically robust supporting substrate, these systems exhibit potential as promising biosensors for the monitoring of wound pH.

Materials

Chitosan (medium molecular weight, 190–310 kDa, 75–85% deacetylated), phosphoryl chloride, dichloromethane (DCM), 1,2-dichloroethane, sodium hydroxide, and triethylamine were purchased from Sigma-Aldrich, Germany. pH 3 buffer (Carl Roth, Germany) and pH 4 buffer (Carl Roth, Germany), both composed of citric acid, NaOH, and NaCl, and pH 10 buffer (Carl Roth, Germany), containing boric acid, NaOH, and KCl, were used. PBS buffer (pH 7.4) was prepared from Milli-Q water (resistivity 18.2 MΩ cm) and biochemistry-grade chemicals (NaCl, KCl, KH_2PO_4, and $Na_2HPO_4{\cdot}2H_2O$, Sigma-Aldrich, Germany). Britton Robinson (BR) buffer was prepared by dissolving H_3PO_4, H_3BO_3, and NaOAc (0.04 M each) in Milli-Q water. Acetic acid (glacial), acetonitrile (MeCN), and *N*-hydroxysuccinimide (NHS) were purchased from Carl Roth, Germany; DMSO and piperidine-4-carboxylic acid were purchased from Fisher Scientific, Germany; and chloroform and ethanol were purchased from VWR Chemicals, Germany. *N*,*N*′-Dicyclohexylcarbodiimide (DCC) was purchased from Fluorochem, UK. Disposable polystyrene Petri dishes (55 × 14 mm) were

purchased from VWR, Germany. Braun Inkjet-F Fine Dosage 1 mL syringes were purchased from Fisher Scientific, Germany. Syringe filters (Chromafil Xtra H-PTFE, 0.45 μm) and filter paper (MN 616, ∅ 150 mm, no. 2) were purchased from Macherey Nagel, Germany. Glass cover slips (22 × 22 mm, #1, Epredia) were purchased from VWR, Germany. 24-well flat-bottom PS plates were purchased from Sarstedt, Germany.

Experimental

The carborhodol dyes AS 14 and AS 15 were synthesized following established procedures (patent EP24200857 filed on 17th September 2024, see the SI for details).[40] The syntheses of AS 14-NHS from AZ 43 and of AS 15-NHS from AZ 129 are shown in Schemes S1 and S2, respectively. The carbopyronine precursors AZ 43 and AZ 129 were synthesized at ATTO-TEC GmbH and used directly for the conversion.[41] The ^{1}H-NMR and ^{13}C-NMR spectra of all synthesized compounds are provided in Fig. S1–S8.

Synthesis of AS 14-NHS

AS 14 was transformed into the NHS ester, AS 14 NHS, *via* reaction with NHS and DCC (Scheme 1). To a stirred solution of AS 14 (45.0 mg, 73.7 μmol) in MeCN (10 mL), at 0 °C, NHS (17.0 mg, 147 μmol) and DCC (31.0 mg, 0.147 mmol) were added one after the other. A precipitate (dicyclohexylurea) formed immediately after the addition of DCC. The ice bath was removed, and the red-colored reaction mixture was stirred for 40 h (HPLC control). Small amounts of NHS and DCC were successively added until complete conversion. The reaction mixture was filtered using a 0.2 μm membrane filter to remove the solids. The filtrate was concentrated under reduced pressure, yielding a red-colored residue, which was redissolved in MeCN (2 mL). AS 14-NHS was precipitated by the addition of diethyl ether/*n*-hexane (1 : 1) and obtained as a red powder (43.0 mg, 72.4 μmol, 98%).

AS 14-NHS HPLC: CH_3CN/H_2O + 0.1 v/v% TFA = 15/85 to 95/5 in 15 min, detection at 550 nm, t_R = 6.5 min (89%).

AS 14-NHS LCMS (ESI^+): *m*/*z* calculated for $C_{35}H_{35}N_3O_6$ $[M + H]^+$: 594.3, found 594.4.

Synthesis of AS 15-NHS

AS 15 was transformed into the NHS ester, AS 15 NHS, *via* reaction with NHS and DCC (Scheme 2). To a stirred solution of AS 15 (35.0 mg, 54.8 mmol) in MeCN (10 mL), at 0 °C, NHS (13 mg, 0.11 mmol) and DCC (23 mg, 0.11 mmol) were added one after the other. A precipitate (dicyclohexylurea) formed immediately after the addition of DCC. The red-colored reaction mixture was stirred for 30 h at r.t. (HPLC control). Small amounts of NHS and DCC were successively added until complete conversion. The reaction mixture was filtered using a 0.2 μm membrane filter to remove the solids. The filtrate was concentrated under reduced pressure, yielding a magenta-colored residue, which was redissolved in MeCN (2 mL). AS 15 NHS was precipitated by the addition of diethyl ether/*n*-hexane (1 : 1) and obtained as a magenta powder (32.0 mg, 51.5 μmol, 94%).

AS 15-NHS HPLC: CH_3CN/H_2O + 0.1 v/v% TFA = 15/85 to 95/5 in 15 min, detection at 550 nm, t_R = 7.4 min (87%).

AS 15-NHS LCMS (ESI^+): *m*/*z* calculated for $C_{37}H_{39}N_3O_6$ $[M + H]^+$: 622.3, found 622.4.

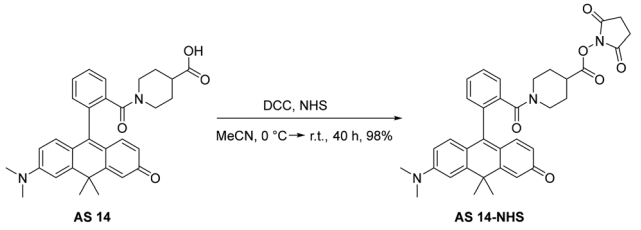

Scheme 1 AS 14-NHS synthesis from AS 14.

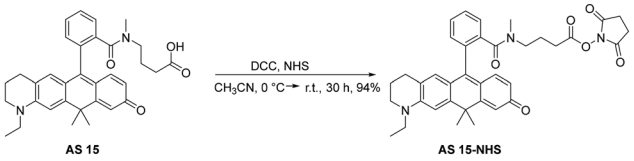

Scheme 2 AS 15-NHS synthesis from AS 15.

Chitosan film preparation

A chitosan (CS) solution was prepared by dissolving medium molecular weight (MMW) CS (1.5 wt%) in 1% acetic acid and stirring overnight at 40 °C. The resulting solution was filtered (∅ = 0.45 μm). To prepare chitosan films, both drop-casting and spin-coating methods were used. For drop-cast films, CS (4 mL) was poured into a PS Petri dish (∅ = 55 mm) and dried overnight in a laminar flow hood to obtain a thin hydrogel film. For spin-coated films, a method adapted from Sadat Ebrahmi *et al.* was used.[42] Briefly, glass cover slips were cut (0.9 × 1.2 cm) and rinsed with chloroform, and then sequentially cleaned three times with ethanol and Milli-Q water. The cleaned cover slips were then dried under a stream of nitrogen and treated with UV-ozone for 30 minutes. CS (300 μL) was added onto pre-cleaned coverslips using a home-built spin coater operated at 2000 rpm for 60 s. The resulting films were annealed in a vacuum oven (40 °C; 5 mbar; 2 hours). Both drop-cast and spin-coated films were neutralized by shaking in NaOH (0.1 M, 5 minutes), rinsed with Milli-Q water (3×), and dried (in a laminar flow hood or under a nitrogen stream).

CS film modification

Dried drop-cast CS films were treated after rehydration in PBS (3.6 mL) either with AS 14-NHS (3 mM) or AS 15-NHS (4 mM) dissolved in DMSO (0.4 mL). The films were incubated for 12 hours under moderate shaking at room temperature. The modified films were then washed with excess PBS on the shaker, replacing the PBS every 30 minutes until no dye was detected in the PBS by UV-Vis spectroscopy. For the modification of spin-coated films, each film was added to a well of a 24-well plate, and the same procedure was followed, but with higher dye concentrations to enable quantification *via* UV-Vis spectroscopy (AS 14-NHS, 14 mM; AS 15-NHS, 20 mM, total

volume 300 μL). Modified spin-coated and drop-cast films were dried under a nitrogen stream.

Estimation of the dye coupling efficiency

After the coupling reaction with drop-cast CS films, the films were washed extensively in Milli-Q (~30 mL) and the washing solution was collected and measured by UV-Vis spectroscopy. Using the Beer–Lambert law, the amount of free dye in this washing solution was calculated (ε = 21 000 M^{-1} cm^{-1} and 52 000 M^{-1} cm^{-1} for AS 14 and AS 15, respectively) and subtracted from the initial amount to calculate the amount of coupled dye. The coupling efficiency was then calculated as the moles coupled *vs.* the initial moles. The degree of functionalization of the free amines of CS was calculated by assuming an average molecular weight of chitosan of 250 kDa and a degree of deacetylation of 75%, which corresponds to 260 μmol free amines per sample. The degree of functionalization was calculated as the moles coupled *vs.* the moles of free amines.

Attenuated total internal reflection-Fourier transform infrared spectroscopy (ATR-FTIR)

The ATR-FTIR spectra of the prepared CS films were recorded using a Tensor 27 Fourier transform infrared spectrometer equipped with a diamond crystal (Bruker Optik GmbH, Germany) over a wavenumber range of 600–4000 cm^{-1} (non-polarized), with a spectral resolution of 4 cm^{-1}. An ambient atmosphere was used to collect the background spectra.

Film thickness determination *via* field emission scanning electron microscopy (FESEM)

The drop-cast films were dried overnight *in vacuo*, sliced with a scalpel, and then attached vertically with carbon tape to a 6-sided metal nut. To create a conductive surface, the samples were sputtered with gold for 30 s, resulting in a ~5.0 ± 0.5 nm thin gold layer. FESEM measurements were obtained using an Inlens secondary electron detector, with an operation voltage of 5 kV (Zeiss Ultra 55cv, Zeiss, Oberkochen, Germany). The images were analyzed using ImageJ software (version 1.54p). To determine the thickness, 3 images per sample were collected, and a mean of diameters measured at 5 points on each separate image was collected. A one-way analysis of variance (ANOVA) test was performed to determine the statistical significance of the thickness of the films *vs.* the non-modified CS film using OriginPro 2018. p values <0.05 were considered statistically significant.

Film thickness determination *via* atomic force microscopy (AFM)

Spin-coated films (3×) were cut (3×) with a sharp metal scalpel, and the step height of the scratch was measured with intermittent contact (tapping) mode AFM (Asylum MFP-3D Bio microscope equipped with a Tap 300 Al-G cantilever from Budget Sensors). This scratch corresponds to the thickness of the film on the Si surface. The measurement was performed under ambient conditions with a resonance frequency of 295 kHz and measured at 80% of the free amplitude. From the AFM images, histograms were plotted showing the pixel height distribution to determine the film thickness.

Swelling ratio determination

The swelling of drop-cast CS films in PBS was investigated. AS 14-CS and AS 15-CS were cut into 2 × 2 cm squares, dried in a vacuum oven (22 °C, 9 mbar) overnight, and weighed (W_i). The films were then immersed in 20.0 mL PBS (pH 7.4, 25 °C) in glass vials, sealed with lids to prevent evaporation, and placed in an incubator at 25 °C. At 60 minute intervals, the samples were carefully removed from the PBS solution, gently dabbed with filter paper to remove excess surface water, and weighed (W_t). This process was repeated for 3 hours, after which time the samples were left in the solution for a total of 19 hours before the final measurement was taken. The gravimetric swelling ratio was calculated using eqn (1). A one-way ANOVA test was performed to determine the statistical significance of the swelling ratio of the modified films *vs.* the non-modified CS film using OriginPro 2018. p values <0.05 were considered statistically significant.

$$\text{Swelling ratio (\%)} = \frac{W_t - W_i}{W_i} \times 100 \quad (1)$$

Determination of the pK_a of free dye in solution

Measuring solutions of AS 14 and AS 15 (20 μM) in BR buffer were prepared by diluting the stock solution (9 mM in DMSO). pH titrations were carried out in BR buffer. The initial absorbance at pH 2.0 was recorded using a 1 cm quartz cuvette. After the initial measurement, the cuvette contents were returned to the bulk pH 2.0 solution, which was then titrated with small aliquots of aq. NaOH (6.2 M) to increase the pH. At each titration step, the cuvette was rinsed with the newly adjusted solution before sample measurement. For each pH point, both pH and UV-Vis absorbance spectra were recorded. The titration was performed in fine increments between pH 2.0 and 7.0 (ΔpH ≈ 0.2), followed by measurements at pH 8.0, 9.0, and 10.0. The pK_a values were obtained from plots of absorbance at a fixed wavelength (corresponding to the λ_{max} of the deprotonated species) against the measured pH values. Numerical fitting of the experimental data to the Henderson–Hasselbalch equation was performed using Origin software.[43]

pK_a determination of dye-modified films

Drop-cast films were immersed in PBS. The resulting hydrated film was placed on a microscope slide (VWR, 76 × 26 mm, thickness 1 mm) with one side of the film taped (Tesa SE) to the slide. For titration, a BR buffer was initially adjusted to pH 9 using NaOH (6.2 M). The film attached to the microscope slide was immersed in the pH 9 buffer for 5 minutes, dried using nitrogen flow, and then placed in the sample holder of a UV-Vis spectrophotometer (PerkinElmer Lambda 750) (Fig. S9). The baseline was measured using a blank microscope slide. All measurements were performed by repositioning the films precisely at a marked location after each treatment.

The pH of the buffer was then gradually decreased in steps of approximately 0.2 pH units by adding small aliquots of HCl (2 M). The films were immersed in each pH sequentially, measuring the absorbance spectra after each immersion.

Absorbance measurements of films

Drop-cast films were attached either to microscope slides (Fig. S9) or in a 35 mm slide mount (Fig. S10), dried using air flow, and the absorption spectra were measured (PerkinElmer Lambda 750 spectrophotometer). Spin-coated films were inserted into a quartz cell with 1 mm path length (SUPRASIL, Hellma Analytics, Germany), and the absorption spectra were measured (Varian Cary 50 Bio spectrophotometer).

Fluorescence turn-on ratio determination

Emission spectra were measured using a Fluorolog 3 spectrofluorometer (HORIBA Jobin Yvon) in a front-face arrangement for the drop-cast films, and in a 90° arrangement with horizontal polarization of emission for the free dye in solution. The films were immersed in a pH 10 buffer, cut into rectangles of 3.0 × 0.9 cm (length × width), and then attached to a quartz cell with a 1 mm path length. After drying using air flow, the spectra were measured (Fig. S11 and S12 for drop-cast and spin-coated films, respectively). The same film was then immersed in a pH 3 buffer, and the process was repeated. To determine the fluorescence turn-on effect, the fluorescence quantum yield (Φ_{fl}) of the basic form of each dye was arbitrarily set to 100, and the quantum yield of the corresponding acidic form was determined relative to this using eqn (2). In this equation, the subscripts "S" and "R" denote the substance under investigation (acidic form) and the reference (basic form), respectively. Int is the integrated fluorescence intensity (area under the emission band), A is the absorbance at the excitation wavelength, and n is the refractive index of the substance. The ratio between the quantum yield of the basic form (100) and that of the acidic form (obtained from eqn (2)) defines the fluorescence enhancement factor, referred to as the fluorescence turn-on ratio.

$$\Phi_S = \Phi_R \times \frac{Int_S}{Int_R} \times \frac{1 - 10^{-A_R}}{1 - 10^{-A_S}} \times \frac{{n_S}^2}{{n_R}^2} \quad (2)$$

Fluorescence lifetime determination of free dye *via* fluorescence lifetime imaging microscopy (FLIM)

The fluorescence lifetimes of the free dyes in solution were measured using a TemPro fluorescence lifetime system from HORIBA Jobin Yvon, employing the time-correlated single photon counting (TCSPC) method. A nano LED serves as the light source, and the excitation was performed using a 562 nm laser source. All measurements were carried out with concentrations leading to an absorbance <0.1 in a 1 cm Hellma fluorescence quartz cuvette. The data were analyzed using bi-exponential fitting, with χ^2 values between 0.900 and 1.200 and evenly distributed residuals taken as criteria for optimal fits. The lifetime of the dominant component was used to describe the decay behavior of the system, while the minor component ($<5\%$ contribution) was considered negligible.

Fluorescence lifetime determination of films *via* FLIM

FLIM was carried out using a Stellaris 8 confocal microscope (Leica Microsystems). Drop-cast films were immersed in corresponding buffer (pH 10 or pH 3 buffer) and cut into small squares ($\sim 0.2 \times 0.2$ cm), attached to microscope slides (VWR, 76 × 26 mm, thickness 1 mm), then flattened using a 10 mm glass coverslip. FLIM images were acquired with an 86×/1.20 water immersion objective at a resolution of 512 × 512 pixels, with excitation wavelengths selected to match the absorption maxima of the respective dye forms (basic form: 590 nm for AS 14-CS and 606 nm for AS 15-CS; acidic form: 520 nm for both films). The relative intensity contributions (f) of each lifetime component were calculated by dividing the photon count (in kilocounts) of each exponential term by the total counts and multiplying by 100.

Color and photostability determination

For the photostability experiments of free dyes, solutions of the corresponding dye samples were prepared in pH 4 or pH 10 buffer such that the extinction at the long-wavelength absorption maximum was approximately 1 in a 1 cm quartz cell. All cuvettes were placed together on an overhead projector (Liesegang Trainer Special HR Electronic Overhead Projector) fitted with a 575 W mercury halide lamp, and the lamp was focused on the cells (Fig. S13). The absorption spectra were recorded at 30-minute intervals for 4 hours and then again after 24 hours. Cuvettes were tightly sealed throughout the experiment.

For photostability experiments of dye-modified films, the drop-cast AS 14-CS and AS 15-CS films were washed with the corresponding buffer (pH 4 or pH 10), attached to a 35 mm slide mount, and placed horizontally on the same overhead projector (Fig. S14). Excess film at the edges was trimmed before positioning the samples. Absorbance measurements were taken every 30 minutes by placing the films directly on the UV-Vis spectrometer sample holder.

Results and discussion

Synthesis of pH-responsive dyes, AS 14 and AS 15

The pH-responsive carborhodol dyes were produced by the alkaline hydrolysis of the corresponding carbopyronines. The direct precursor carbopyronine compound is dissolved in an aqueous hydroxide solution. Organic solvents, such as ethanol, methanol, acetone, or acetonitrile, can be used as co-solvents to enhance the solubility of the reactants. The reaction time depends on the concentration of the reactants (precursor and alkali) and the temperature. The best results were obtained with temperatures between 50 and 90 °C. The only prerequisite for this simple one-step reaction is the presence of a dimethylamino group, at least at one terminal end of the chromophoric system of the parent carbopyronine compound.

Using this synthetic approach, carbopyronines AZ 43 and AZ 129 (both synthesized at ATTO-TEC GmbH) were treated with a 1 : 1 mixture of 2.5 M aq. NaOH and ethanol at 85 °C and were successfully converted into the corresponding carborhodol

derivatives AS 11 in 68% yield (Scheme S1) and AS 12 in 54% yield (Scheme S2), respectively. AS 11 corresponds to a previously reported compound described by Sednev *et al.*[38,41] Compared to their approach, the alkaline hydrolysis approach enabled the simultaneous production of two valuable dyes: the precursor carbopyronine and the product carborhodol.

To prevent the formation of the colorless spirolactone form, often undesirable for fluorescence applications, the *ortho*-carboxylic acid groups of AS 11 and AS 12 were further functionalized. Specifically, AS 11 was modified using piperidine-4-carboxylic acid to yield AS 14 (Scheme S1), while AS 12 was derivatized with methyl 4-(methylamino)butanoate to give AS 15 (Scheme S2) (patent filed).[40] Multiple attempts to directly generate active esters from AS 11 and AS 12 were unsuccessful. Consequently, these elongations were carried out *via* the corresponding acid chloride intermediates. The resulting elongated compounds AS 14 and AS 15 were then converted into their respective active esters *via* reaction with NHS and DCC (Schemes 1 and 2).

Coupling of carborhodol dyes to chitosan films

The pH-responsive chitosan-based hydrogel films were prepared by covalently attaching the NHS ester-activated carboxylic groups of the carborhodol dyes, AS 14 and AS 15, to the primary amine groups of the glucosamine units in chitosan *via* amide bond formation (Scheme 3).

Colored and fluorescent films were successfully prepared using both drop-casting and spin-coating techniques. Given the greater potential of drop-cast films for practical applications in wound dressings due to a lack of support material, their characterization is presented here, while the photophysical data for spin-coated films are provided in the SI (Fig. S15 and S16).

To determine the successful coupling of the NHS esters to the chitosan backbone, the films formed were washed excessively in Milli-Q water until no free dye was detected *via* absorption spectroscopy in the surrounding media. To estimate the maximum amount of dye within the CS matrix, the moles of unbound free dye were calculated from the absorption spectra

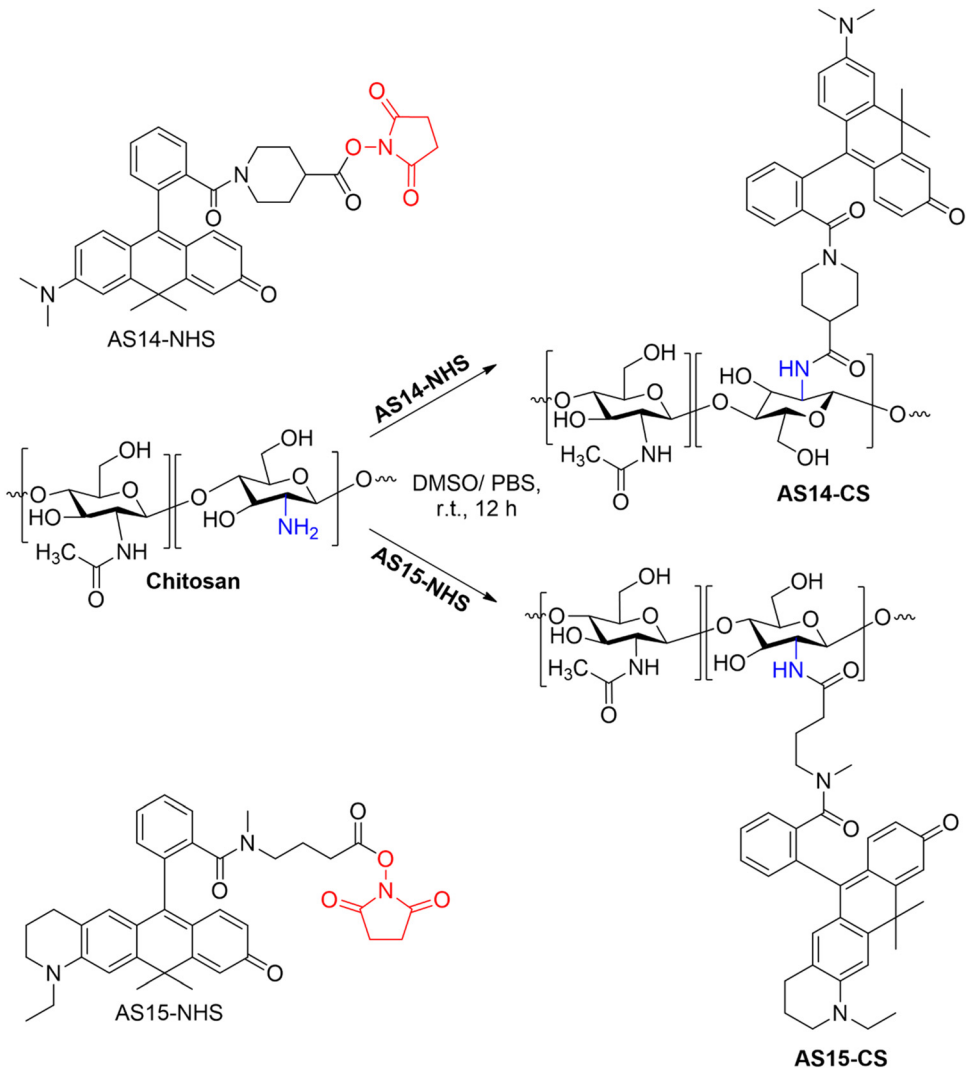

Scheme 3 Covalent modification of chitosan films *via* coupling with NHS-esters of pH-sensitive carborhodol dyes, AS 14 and AS 15.

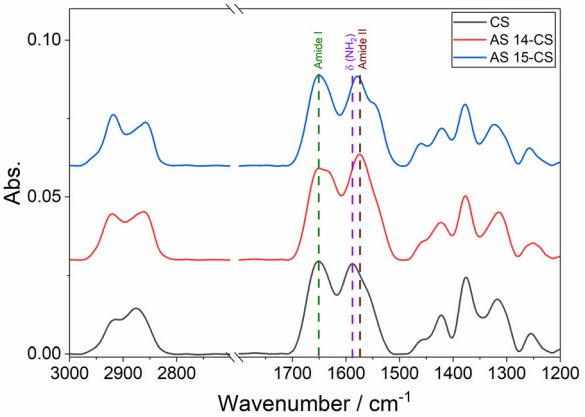

Fig. 1 ATR-FTIR spectra of non-modified CS, AS 14-CS, and AS 15-CS.

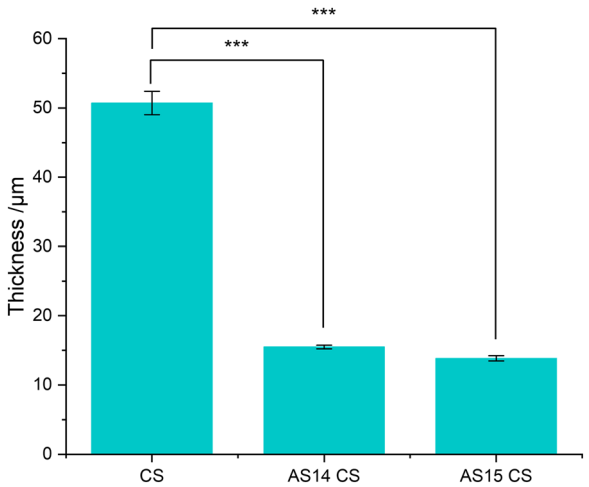

Fig. 2 Bar chart of the average film thickness for non-modified CS, AS 14-CS and AS 15-CS films, determined by FESEM. Asterisks represent significant difference from non-modified CS (***: $p < 0.001$).

and subtracted from the initial amount of dye added, equating to 36.3% and 66.6% for AS 14-CS and AS 15-CS, respectively. The maximum degree of functionalization was calculated to be 0.16% and 0.41% for AS 14-CS and AS 15-CS, respectively.

ATR-FTIR measurements were then recorded to confirm amide bond formation (Fig. 1). The disappearance of the band at 1588 cm^{-1}, typically attributed to the primary amine group of the glucosamine unit in chitosan, suggests its involvement in a chemical reaction. The increased intensity of the band at 1650 cm^{-1}, corresponding to amide I (C═O) vibrations, indicates the formation of new amide bonds. Additionally, a band at 1630 cm^{-1} observed in AS 14-CS, likely arising from both the dye's inherent tertiary amide and new amide linkages, further supports the generation of amide I. Enhanced intensities near 1570 cm^{-1} for both AS 14-CS and AS 15-CS, and the appearance of a new band at 1546 cm^{-1} in AS 15-CS, characteristic of amide II (N–H), support the conclusion that amino groups participated in covalent bonding through the formation of secondary amide linkages. The assignment of the observed bands is summarized in Table S1.

To further confirm the successful conjugation of the dyes to the chitosan backbone, the films were immersed in different media (water and EtOH/water 1 : 1) at room temperature. The films were stable and able to maintain their color in each medium even after seven months (Fig. S17). In addition, the UV-Vis spectra of the solutions used for immersing films were measured after 24 h, and the absorption bands corresponding to the leaching dyes were not detected, confirming that covalently attaching dyes onto CS avoids dye release or degradation of the film color (Fig. S17). These data therefore provide confirmation of a stable dye-coupled chitosan film.

Film thickness

The dry film thickness of spin-coated chitosan films was measured by atomic force microscopy (AFM). Films were placed in the AFM and analysed under ambient atmosphere, and a scratch through the polymer layer to the silicon surface was created with a scalpel. The step height across the scratch was measured, corresponding to the CS film layer thickness. As expected, the films were observed to increase in thickness upon dye modification, with the blank film showing a thickness of 195 ± 3 nm, while AS 14-CS and AS 15-CS films exhibited significantly ($p = 0.001$) increased thicknesses of 239 ± 4 nm and 252 ± 4 nm, respectively (Fig. S19).

In contrast, the dry film thickness of drop-cast chitosan films, as analyzed by FESEM, showed the opposite behavior. The non-modified chitosan film exhibited a thickness of 50.7 ± 1.7 µm, whereas covalent modification with NHS ester-functionalized dyes resulted in a significant ($p = 0.001$) reduction to 15.5 ± 0.3 µm and 13.8 ± 0.4 µm for AS 14-CS and AS 15-CS films, respectively, indicating a denser and more compact hydrogel structure (Fig. 2 and Fig. S18). While this difference in thickness could be in parts due to the projection angle in the FESEM, the results were consistent across samples. This is therefore likely to indicate a more compact structure due to interactions between the dye and the CS.

Swelling behavior

The gravimetric swelling ratio of the chitosan films was evaluated to assess their water uptake capacity. As shown in the swelling profile (Fig. 3), all films exhibited the ability to absorb water up to approximately 200% of their dry weight. The maximum swelling was observed within the first hour, after which no significant changes occurred, indicating equilibrium swelling behavior. Notably, both the non-modified chitosan film and the dye-modified films (AS 14-CS and AS 15-CS) demonstrated similar gravimetric swelling ratios ($p > 0.05$), suggesting that the modification did not adversely affect the swelling capacity of the polymer. This high gravimetric swelling ratio is advantageous for wound dressing applications, as it would enable the maintenance of a moist wound environment, facilitating the wound-healing process.

pH sensitivity

As shown in Fig. 4, the color difference between the acidic and basic forms of chitosan-based films in response to changes in the surrounding media is clearly visible to the naked eye. Upon

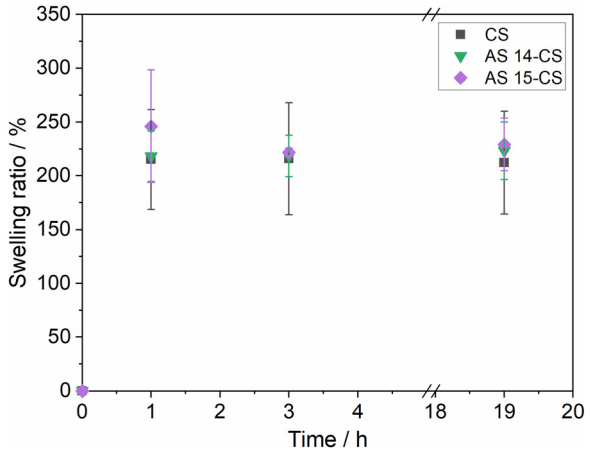

Fig. 3 Swelling ratios of non-modified CS, AS 14-CS, and AS 15-CS in PBS (25 °C).

exposure to pH 4 buffer, both films immediately changed to pink. When washed with pH 8 buffer, the films turned to the characteristic color of the basic form of each dye; purple for AS 14-CS and blue for AS 15-CS. This reversible color change confirms that both films function as chromogenic (colorimetric) pH indicators, based on their pH-dependent structural change. Under UV illumination at 366 nm, the AS 14-CS film exhibited a pronounced fluorescence turn-on response when transitioning from pH 4 to pH 8. This fluorescence enhancement is readily observable by the unaided eye, as the film appears significantly brighter at pH 8 compared to pH 4. This behavior is consistent with the photophysical response of the free AS 14 dye, which shows a fluorescence turn-on ratio of 29 between acidic and basic conditions. Therefore, AS 14 can be employed as both a colorimetric and fluorogenic pH sensor. In contrast, the AS 15-CS film showed only a minor increase in fluorescence intensity, corresponding to the relatively low turn-on ratio of the free AS 15 dye (1.7).

pK_a determination

The pH-dependent absorption properties of the neat dye (free dye) in solution and of the modified drop-cast chitosan films were investigated by photometric acid–base titrations in Britton–Robinson buffer over the pH range 2.0–10.0 (Fig. 5).

For the free dyes in solution, at acidic pH (pH 2), both AS 14 and AS 15 exhibited a broad absorption band centered at 515 nm that can be attributed to the protonated species. The full width at half maximum (FWHM) was 100 nm for AS 14 and 104 nm for AS 15. With increasing pH, this band gradually decreased in intensity, while a new, sharper band of higher molar absorptivity appeared at 586 nm (AS 14, FWHM: 41 nm) and 599 nm (AS 15, FWHM: 35 nm), consistent with the formation of the deprotonated form. This spectral change was accompanied by a distinct visible color shift from pink to violet for AS 14 and from pink to blue for AS 15. In both cases, the absorption spectra recorded at intermediate pH values displayed a well-defined isosbestic point (549 nm for AS 14 and 553 nm for AS 15), confirming a clean equilibrium between the protonated (acidic) and deprotonated (basic) forms (Fig. 5). For both dyes, the absorption at λ_{max} of the deprotonated form was plotted against the pH value of the solution, and the experimental data were analyzed by fitting to the theoretical model for weak acids (Henderson–Hasselbalch), yielding pK_a values of 5.7 for AS 14 and 6.3 for AS 15.[43]

For the modified CS films, titrations were carried out over a pH range of 4.0 to 10.0. When the pH reached 3, the films tended to detach from the slide, making further measurements difficult, likely due to partial solubilization of the chitosan matrix under acidic conditions. In contrast, at pH values above 3, the films remained stable and adhered well to the glass surface. However, a single brief washing in pH 3 buffer followed by immediate measurements was still feasible. For the AS 14-CS film, the absorption spectrum at acidic pH (pH 4) shows a broad band (FWHM: 132 nm) centered at 520 nm (red trace), corresponding to the protonated form of the dye. As the pH increases, the intensity of this band gradually decreases, while a narrower band (FWHM: 67 nm) at 590 nm (blue trace), attributed to the deprotonated form of the dye, emerges with higher molar absorptivity. A bathochromic shift of approximately 4 nm is observed for both the acidic and basic forms compared to the free dye in solution. Similar bathochromic

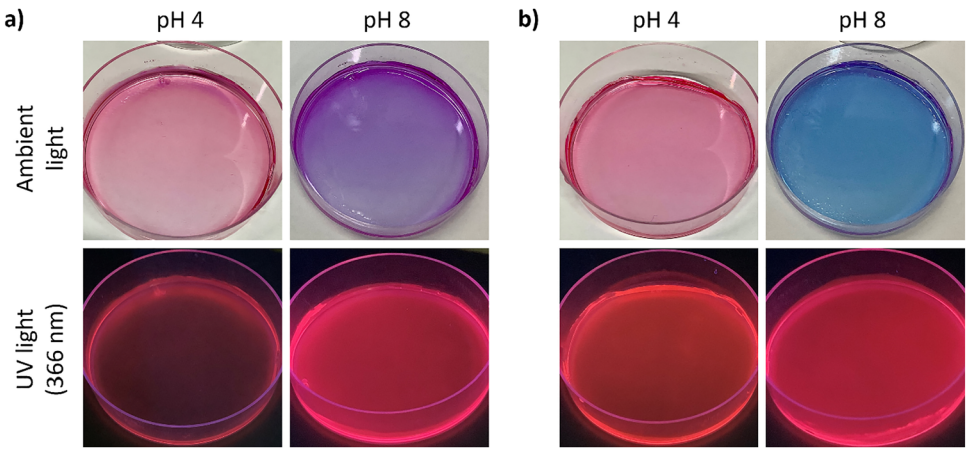

Fig. 4 Photographs of (a) AS 14-CS and (b) AS 15-CS films at pH 4 and pH 8, under ambient and UV light (366 nm).

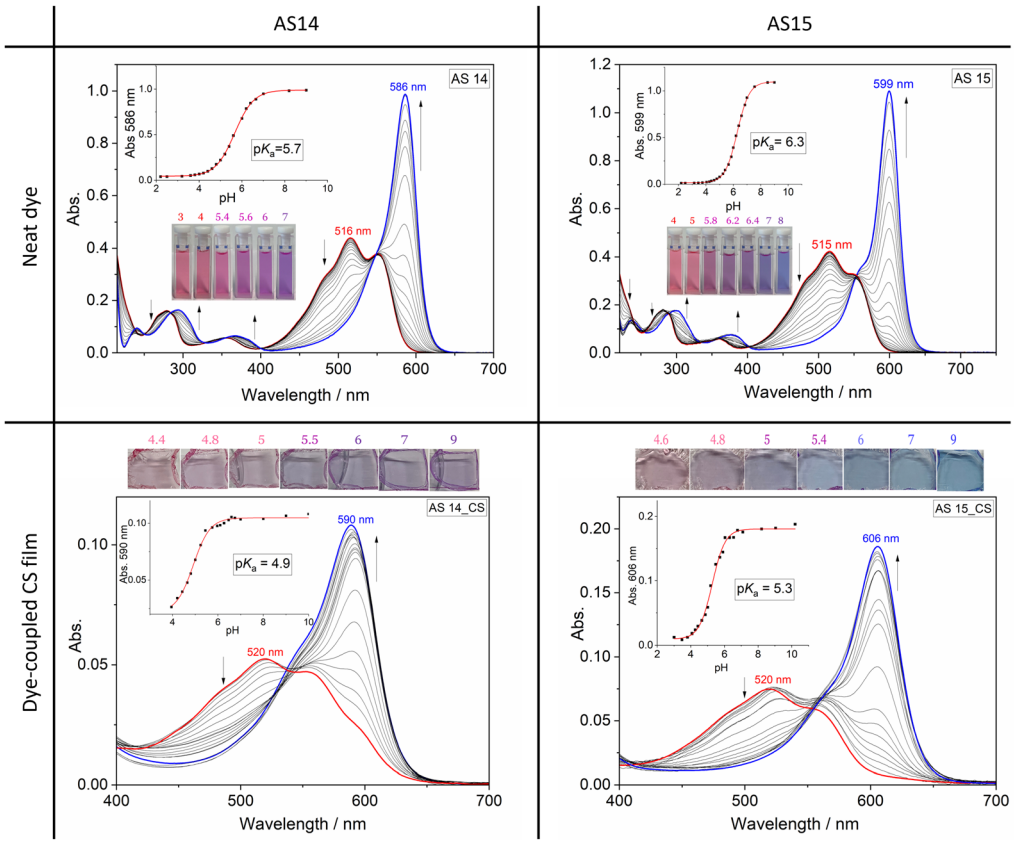

Fig. 5 pH-Dependent absorption spectra of AS 14 and AS 15 in solution and coupled to CS films. Arrows indicate the development of bands with increasing pH value of the solution. Insets show the absorbance at long wavelength absorption maxima as a function of pH. The red line denotes the best fit of the experimental data to the theoretical isotherm of a weak acid; pK_a is determined from this plot. Photographs show the visual appearance of samples at the indicated pH values.

shifts have been observed upon conjugation of other dyes such as fluorescein and rhodamine isothiocyanate to chitosan, attributed to the change from the solution to the solid state.[44,45] This spectral shift with pH change is accompanied by a visible color change from pink (acidic) to violet (basic). The spectra exhibit an isosbestic point at approximately 540 nm, indicating a clean two-state equilibrium between the protonated and deprotonated species. The absorption at λ_{max} = 590 nm was plotted against the pH value of the solution, yielding a pK_a value of 4.9 (Fig. 5).[43]

In the case of AS 15-CS, the protonated form exhibits a broad absorption band (FWHM: 113 nm) centered at 520 nm, while the deprotonated form gives rise to a narrow band (FWHM: 51 nm) at 606 nm. Compared to the free dye, bathochromic shifts of 5 nm (acidic form) and 7 nm (basic form) were observed upon immobilization onto the chitosan hydrogel. The spectra display an isosbestic point at around 550 nm. A gradual change from pink to blue is visually observed as the pH increases. The pK_a value for AS 15-CS was determined to be 5.3, based on a sigmoidal fit of the absorbance at 606 nm *versus* pH. The chemical changes of the dyes from acidic to basic forms are exhibited in Scheme 4.

In both cases, the pK_a values of the CS-bound dyes were approximately one pH unit lower than those of the corresponding

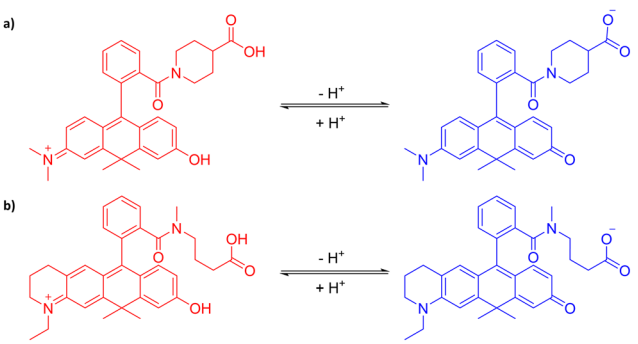

Scheme 4 Protonation–deprotonation equilibria of (a) AS 14 and (b) AS 15. Structures shown in red correspond to the protonated forms, while structures in blue represent the deprotonated forms.

free dyes in solution. The observed decrease in the pK_a of the dye upon immobilization in the chitosan film is likely due to several microenvironmental effects. These effects could include hydrogen bonding between the hydroxyl groups of CS and the deprotonated dye, which stabilizes the conjugate base. Thus, with increased stability of D^-, K_a increases and pK_a decreases (eqn (3)).

$$K_a = \frac{[D^-][H_3O^+]}{[DH]} \quad (3)$$

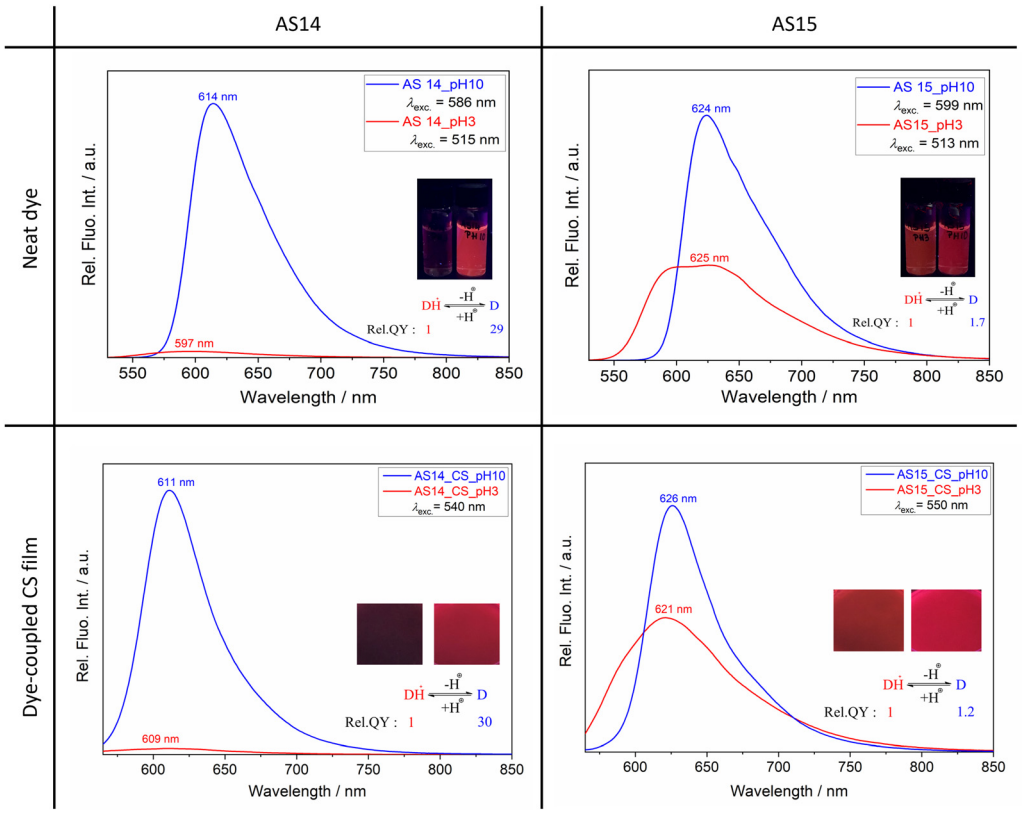

Fig. 6 Fluorescence emission spectra of AS 14 and AS 15 in solution and coupled to CS films recorded in aqueous buffer at pH 10 (blue trace) and pH 3 (red trace). The free dyes (AS 14 and AS 15) in solution were excited at their respective absorption maxima, while the chitosan-coupled dyes (AS 14-CS and AS 15-CS) were excited at their isosbestic points. Insets show photographs of the corresponding dye solutions and films at pH 3 (left) and pH 10 (right).

Fluorescence turn-on ratio

As observed in Fig. 4, the fluorescence intensity of the chitosan films is higher in a basic environment compared to acidic conditions. To quantify this difference, fluorescence turn-on ratios were calculated. For the CS-films, both the acidic and basic forms were excited at their respective isosbestic points, which are the wavelengths at which both forms exhibit equal absorbance (*i.e.*, 540 nm for AS 14-CS and 550 nm for AS 15-CS). The free dye in solution was excited at its respective absorption maximum corresponding to either the acidic or the basic form. To ensure comparability, the absorbance at the chosen excitation wavelength was adjusted to be identical for both protonation states (for AS 14: 515 nm for the acidic form and 586 nm for the basic form; for AS 15: 513 nm for the acidic form and 599 nm for the basic form). The turn-on ratios observed for the chitosan-bound dyes were comparable to those of the free dyes in solution. Specifically, AS 14-CS exhibited a fluorescence turn-on ratio of 30, closely matching that of the free dye (29), while AS 15-CS showed a lower turn-on ratio of 1.2, also comparable to its free dye counterpart (1.7) (Fig. 6). The modified films exhibited emission wavelength variations of 2–4 nm, except for the AS 14-CS acidic film, which showed a 12 nm bathochromic shift compared to the free dye in solution.

Fluorescence lifetimes

The fluorescence lifetime of the dye-coupled films was measured using fluorescence-lifetime imaging microscopy (FLIM), employing time-correlated single-photon counting (TCSPC). The time-dependent fluorescence decay, $A(t)$, can be described as a sum of exponential functions (eqn (4)), where τ_i and a_i are the lifetime and amplitude of the ith component, respectively, and t is the time variable.

$$A(t) = \sum_i a_i \times \exp\left(\frac{-t}{\tau_i}\right) \quad (4)$$

The resulting lifetime components (τ), their relative intensity contributions (f), average lifetime ($\langle\tau\rangle$), and free dye lifetimes in buffer are given in Table 1.

The films were washed in pH 10 and pH 3 buffer to obtain basic and acidic conditions, respectively. In their basic forms,

Table 1 Fluorescence lifetime components (τ), relative intensity contributions (f), average lifetime ($\langle\tau\rangle$), and reference lifetimes of the corresponding free dyes in buffer

Sample	τ_1 (ns)	f_1 (%)	τ_2 (ns)	f_2 (%)	$\langle\tau\rangle$	Free dye τ (ns)
AS 14-CS (b)	1.1	5.0	3.3	95	3.2	2.3
AS 14-CS (a)	0.1	46	0.9	54	0.5	0.2
AS 15-CS (b)	0.7	2.0	3.5	98	3.5	2.7
AS 15-CS (a)	1.1	23	2.7	77	2.3	1.6

(a) and (b) correspond to acidic and basic forms, respectively. The quality of the bi-exponential fit was assessed using reduced χ^2 values and the distribution of weighted residuals.

the AS 14-CS and AS 15-CS films exhibit dominant lifetime components of 3.29 ns (95%) and 3.54 ns (98%), respectively, with the shorter-lived components contributing negligibly to the overall decay. In their acidic forms, the shorter-lived component contributes more significantly to the overall lifetime. In the weakly emissive AS 14-CS acidic form, two distinct lifetime components were evident, indicating the presence of multiple emissive states, which is consistent with its lower pK_a (4.9), where small variations in pH can significantly affect protonation equilibrium and thus modulate the dye's excited-state behavior. For the acidic form of AS 15-CS, although a second component was present, the average lifetime remained close to the dominant component, suggesting that the contribution of the secondary species is less pronounced.

Both AS 14 and AS 15 exhibited increased fluorescence lifetimes upon incorporation into chitosan films, in both their acidic and basic forms, compared to their free counterparts in aqueous buffer. This enhancement in lifetime is consistent

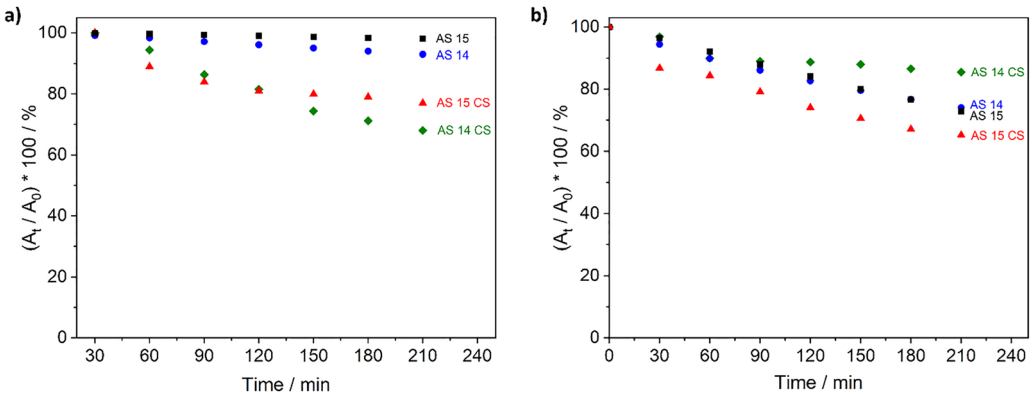

Fig. 7 Photostability profiles of (a) the acidic form and (b) the basic form of the free dyes and chitosan-coupled dyes in pH 4 and pH 10 buffers, respectively, over 3.5 hours of continuous irradiation using a 575 W mercury halide lamp.

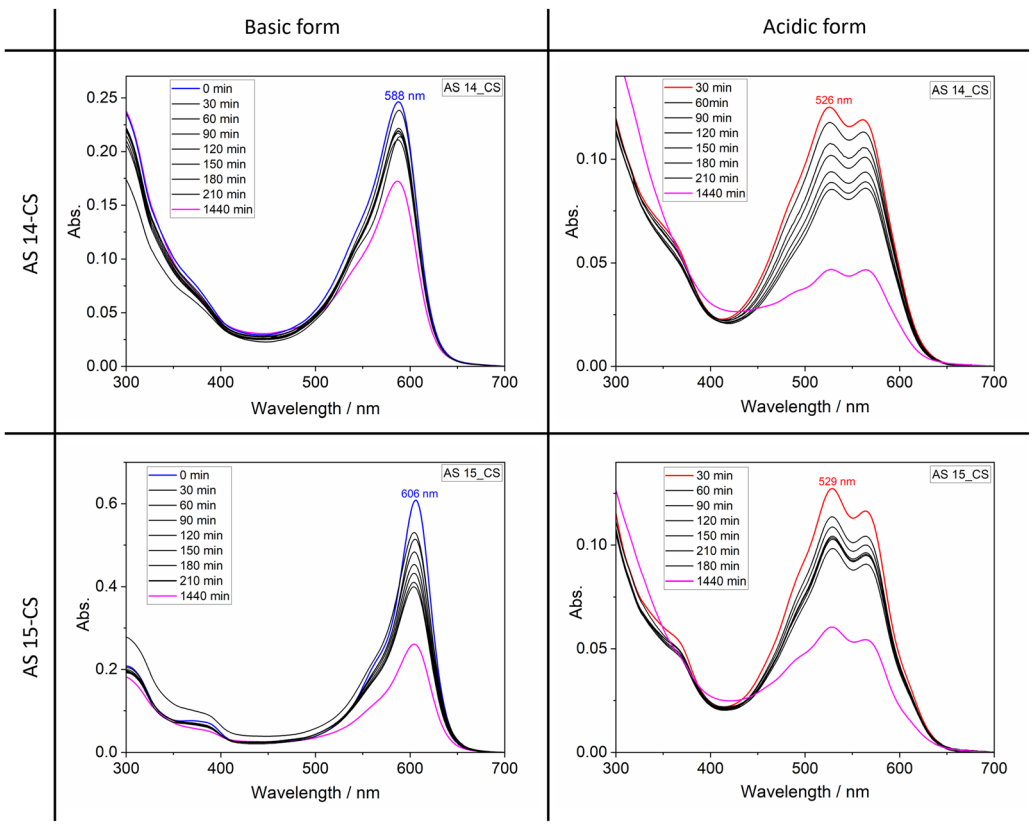

Fig. 8 Change in absorption spectra over time for AS 14-CS and AS 15-CS in basic and acidic forms under continuous irradiation using a 575 W mercury halide lamp.

with previous observations in chitosan-based polyelectrolyte complexes doped with xanthene dyes such as eosin Y and erythrosin B, where changes in the local microenvironment, particularly polarity, influenced the lifetime.[46] Both AS 14 and AS 15 are known to demonstrate solvent-dependent lifetime behavior, with longer lifetimes observed in polar organic solvents relative to aqueous buffer (Table S2). When covalently bound to chitosan, the dye experiences changes in the polarity of its surroundings, resulting in a longer lifetime. Nevertheless, consistent with the behavior observed for the free dyes in solution, the basic form continued to display a longer lifetime than the acidic form in the chitosan films.

Importantly, these pH-responsive color and fluorescence changes are studied here only in controlled buffered solutions that mimic the pH changes observed in infected wounds. For future application as an infection-sensing substrate, these properties must be later investigated in relevant media.

Color and photostability

The color stability of pH-sensitive films relies on the choice of dyes. Dyes like anthocyanin and alizarin tend to degrade quickly when exposed to heat and light.[47,48] To maintain their color, these films should be stored at reduced temperatures and protected from light. Moreover, dyes that are incorporated into polymers without covalent bonds may leach out over time.[47,49] Therefore, it is necessary to assess the color and photostability of the pH-sensitive films.

To evaluate the photostability of the dyes when immobilized, the acidic and basic forms of the AS 14-CS and AS 15-CS films, as well as the free dyes in solution, were irradiated under identical conditions using a 575 W mercury halide lamp. The photostability of the free dye and dye-coupled films was then assessed by monitoring the decrease in absorbance at λ_{max} over time under continuous illumination (Fig. 7).

Compared to the standard indicator fluorescein and the common biological label Cy5, carborhodols display superior photostability, addressing a key limitation of existing probes (Fig. S20). The free dyes AS 14 and AS 15 demonstrated excellent photostability in their acidic forms, with only 7% and 2% degradation, respectively, after 210 minutes of continuous irradiation (Fig. 7a). When immobilized in chitosan films, AS 14-CS and AS 15-CS exhibited higher degradation rates under the same conditions, at 32% and 23%, respectively (Fig. 8).

Under basic conditions, the free dyes showed greater photodegradation, with both AS 14 and AS 15 displaying approximately 26% loss in absorbance (Fig. 7b). In contrast, AS 14-CS was the most photostable among all tested systems under basic conditions, exhibiting only 15% degradation, while AS 15-CS showed a higher degradation of 35%. All these values still indicate good photostability of the film, considering the harsh experimental conditions compared to the normal wound environment.

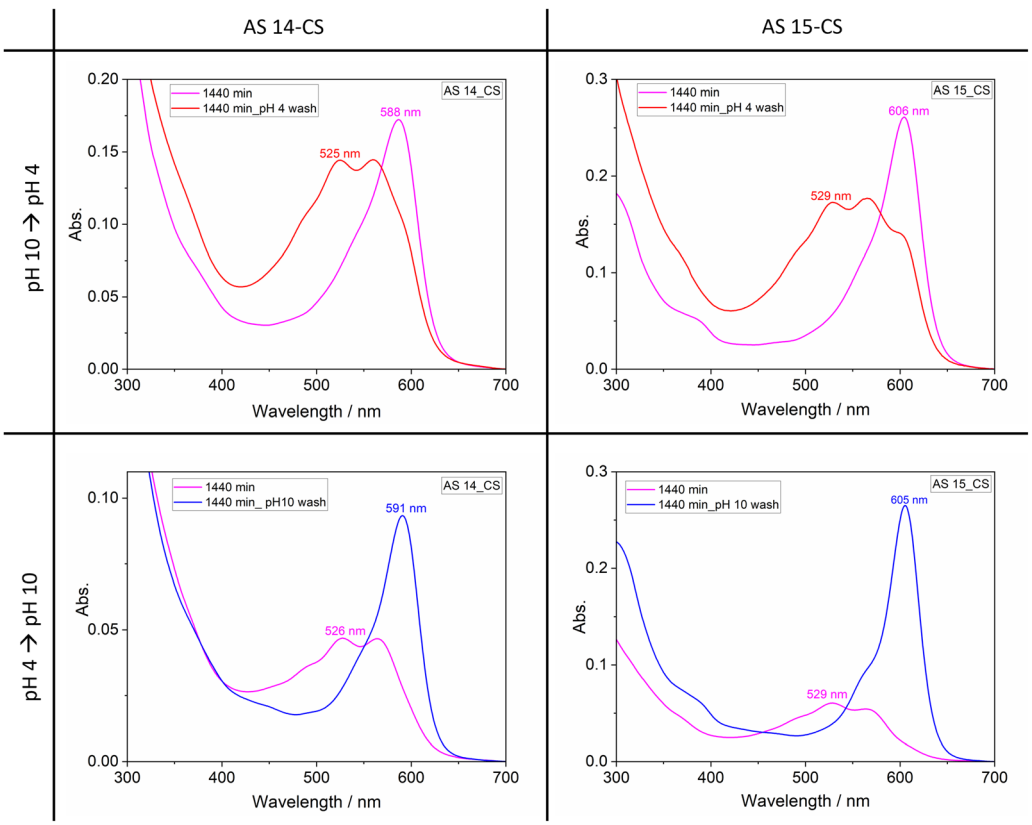

Fig. 9 Absorption spectra of AS 14-CS and AS 15-CS films irradiated in the basic or acidic form for 24 hours, then immersed in a buffer of pH 4 or pH 10, respectively, and dried.

To determine whether films are still sensitive to pH changes after irradiation, films exposed to 24 hours of continuous irradiation were immersed in buffers of different pH values, and the absorption spectra measured. When irradiated basic films were washed with pH 4 buffer, they exhibited a visible color change to pink, consistent with the protonated (acidic) form of the dye. Conversely, rinsing with pH 8 buffer restored the characteristic color of the deprotonated (basic) form in the acidic films. Subsequent spectral measurements confirmed that these washed films displayed absorption profiles corresponding to their respective acidic and basic forms (Fig. 9). As a control, a blank chitosan film without dye was measured under the same irradiation and buffer conditions, and no spectral changes were observed (Fig. S21), confirming the stability of the chitosan matrix.

Conclusions

pH-responsive wound dressing-type materials were developed by covalently coupling NHS-esters of novel photostable carborhodol dyes, AS 14 and AS 15 to CS films. The coupling was successfully achieved for CS films prepared *via* drop-casting on polystyrene and spin-coating on glass, as confirmed by ATR-FTIR spectroscopy, UV-VIS absorption, and fluorescence measurements. This amide bond formation affords non-leaching pH-sensing biopolymer films. Both AS 14-CS and AS 15-CS exhibited distinct and reversible color changes within the clinically relevant pH range of 4–7, with pK_a values of 4.9 and 5.3, respectively. In the basic form, the fluorescence intensity was enhanced compared to the acidic form, with turn-on ratios of 30 for AS 14-CS and 1.2 for AS 15-CS.

The reported AS 15-CS film functions primarily as a chromogenic sensor, with clear color changes from pink to blue to indicate infection-associated pH elevation. The developed AS 14-CS film exhibits both chromogenic and fluorogenic responses, enabling pH monitoring by the naked eye, with a pink-to-purple color change under ambient light or a significant increase in fluorescence intensity under UV illumination. AS 14-CS could therefore be used as an efficient monitor of wound infection status.

Both films showed pH-dependent fluorescence lifetimes, with longer lifetimes in basic and shorter in acidic states. This is particularly advantageous to distinguish between any potential autofluorescence of biological tissue and the dye itself, while also introducing the possibility of FLIM monitoring of wound status. The materials demonstrated high photostability, color stability, resistance to dye leaching in aqueous and mixed solvent systems, a gravimetric swelling ratio of approximately 200%, and maintained reversible optical responses after prolonged irradiation. In addition, a shelf-life of $\geq$7 months and the stability of the films in ethanolic solutions for sterilization make these materials particularly attractive. Collectively, these results highlight a novel, simple, and efficient strategy for fabricating stable, pH-responsive wound dressings capable of real-time visual and fluorescence-based monitoring of wound status.

To further develop these systems towards clinical applicability, additional characterization under wound-relevant conditions is required. This includes *in vitro* evaluation in simulated wound fluid in the presence of bacteria, followed by *ex vivo* studies using porcine skin models and ultimately validation in *in vivo* wound models.

Author contributions

The manuscript was written through the contributions of all authors. All authors have given approval to the final version of the manuscript.

Conflicts of interest

European patent EP24200857 filed on 17th September 2024.

Abbreviations

CS	Chitosan
MMW	Medium molecular weight
BR buffer	Britton Robinson buffer
DCC	*N*,*N*′-Dicyclohexylcarbodiimide
MeCN	Acetonitrile
DCM	Dichloromethane
PBS	Phosphate-buffered saline
NHS	*N*-Hydroxysuccinimide
TFA	Trifluoroacetic acid
DMSO	Dimethylsulfoxide
NaOH	Sodium hydroxide
FWHM	Full width at half maximum
TCSPC	Time-correlated single photon counting
FLIM	Fluorescence lifetime imaging microscopy
AFM	Atomic force microscopy
FESEM	Field emission scanning electron microscopy
ANOVA	Analysis of variance
ATR-FTIR	Attenuated total internal reflection-Fourier transform infrared
HPLC	High-performance liquid chromatography
LCMS	Liquid chromatography-mass spectrometry
NMR	Nuclear magnetic resonance

Data availability

In addition to selected data in the supplementary information (SI), the research data associated with the paper will be made available after acceptance of the manuscript in the open access depository Zenodo. Supplementary information: additional experimental results, including synthesis of AS 14 and AS 15, absorption and emission spectra, AFM micrographs of spin-coated films, ATR-FTIR band assignments, absorption spectra of unmodified CS films upon irradiation, UV-Vis spectra confirming lack of leaching, and images of the experimental setup for spectroscopic measurements (PDF). See DOI: https://doi.org/10.1039/d6ma00022c.

Acknowledgements

This project (STIMULUS) has received funding from the EU's Horizon 2020 Research and Innovation program under the Marie Skłodowska-Curie Actions grant agreement no. 955644. The authors would like to thank Prof. Dr Xin Jiang for access to the FESEM, Prof. Dr Ulrich Jonas for access to the FTIR spectrometer, Winny Chelangat for FESEM measurements, Dr Jan Erik Hoffmann for FLIM measurements, Joshua Schumacher for AFM measurements and Dr Stephan Schandl for insightful discussions. Part of this work was performed at the DFG-funded Micro- and Nanoanalytics Facility (MNaF) of the University of Siegen (INST 221/131-1).

References

1 K. Bumpus and M. A. Maier, The ABC's of wound care, *Curr. Cardiol. Rep.*, 2013, **15**, 346.
2 S. Raoofi, F. Pashazadeh Kan, S. Rafiei, Z. Hosseinipalangi, Z. Noorani Mejareh, S. Khani, B. Abdollahi, F. Seyghalani Talab, M. Sanaei and F. Zarabi, *et al.*, Global prevalence of nosocomial infection: A systematic review and meta-analysis, *PLoS One*, 2023, **18**, e0274248.
3 J. Dissemond, J.-D. Rembe, B. Assenheimer, M. Barysch-Bonderer, V. Gerber, J. Kottner, P. Kurz, M. Motzkus, E.-M. Panfil and S. Probst, *et al.*, Systematics, diagnosis and treatment of wound infections in chronic wounds: A position paper from WundDACH, *J. Dtsch. Dermatol. Ges.*, 2025, **23**, 565–574.
4 T. Swanson, K. Ousey, E. Haesler, T. Bjarnsholt, K. Carville, P. Idensohn, L. Kalan, D. H. Keast, D. Larsen and S. Percival, *et al.*, IWII Wound Infection in Clinical Practice consensus document: 2022 update, *J. Wound Care*, 2022, **31**, S10–S21.
5 M. Falcone, B. D. Angelis, F. Pea, A. Scalise, S. Stefani, R. Tasinato, O. Zanetti and L. Dalla Paola, Challenges in the management of chronic wound infections, *J. Global Antimicrob. Resist.*, 2021, **26**, 140–147.
6 R. B. Blankenship and T. Baker, Imaging modalities in wounds and superficial skin infections, *Emerg. Med. Clin. N. Am.*, 2007, **25**, 223–234.
7 C. Wang, E. Shirzaei Sani, C.-D. Shih, C. T. Lim, J. Wang, D. G. Armstrong and W. Gao, Wound management materials and technologies from bench to bedside and beyond, *Nat. Rev. Mater.*, 2024, **9**, 550–566.
8 A. Pusta, M. Tertiş, C. Cristea and S. Mirel, Wearable Sensors for the Detection of Biomarkers for Wound Infection, *Biosensors*, 2021, **12**, 1.
9 S. Haas, N. Hain, M. Raoufi, S. Handschuh-Wang, T. Wang, X. Jiang and H. Schönherr, Enzyme degradable polymersomes from hyaluronic acid-*block*-poly(ε-caprolactone) copolymers for the detection of enzymes of pathogenic bacteria, *Biomacromolecules*, 2015, **16**, 832–841.
10 J. Zhou, D. Yao, Z. Qian, S. Hou, L. Li, A. T. A. Jenkins and Y. Fan, Bacteria-responsive intelligent wound dressing: Simultaneous In situ detection and inhibition of bacterial infection for accelerated wound healing, *Biomaterials*, 2018, **161**, 11–23.
11 O. Simoska, J. Duay and K. J. Stevenson, Electrochemical Detection of Multianalyte Biomarkers in Wound Healing Efficacy, *ACS Sens.*, 2020, **5**, 3547–3557.
12 Q. Alhusaini, W. S. Scheld, Z. Jia, D. Das, F. Afzal, M. Müller and H. Schönherr, Bare Eye Detection of Bacterial Enzymes of Pseudomonas aeruginosa with Polymer Modified Nanoporous Silicon Rugate Filters, *Biosensors*, 2022, **12**, 1064.
13 Z. Jia, M. Müller, T. Le Gall, M. Riool, M. Müller, S. A. J. Zaat, T. Montier and H. Schönherr, Multiplexed detection and differentiation of bacterial enzymes and bacteria by color-encoded sensor hydrogels, *Bioact. Mater.*, 2021, **6**, 4286–4300.
14 C. Deusenbery, Y. Wang and A. Shukla, Recent Innovations in Bacterial Infection Detection and Treatment, *ACS Infect. Dis.*, 2021, **7**, 695–720.
15 J. R. Sharpe, S. Booth, K. Jubin, N. R. Jordan, D. J. Lawrence-Watt and B. S. Dheansa, Progression of wound pH during the course of healing in burns, *J. Burn Care Res.*, 2013, **34**, e201–e208.
16 L. A. Schneider, A. Korber, S. Grabbe and J. Dissemond, Influence of pH on wound-healing: a new perspective for wound-therapy?, *Arch. Dermatol. Res.*, 2007, **298**, 413–420.
17 E. Proksch, pH in nature, humans and skin, *J. Dermatol.*, 2018, **45**, 1044–1052.
18 R. Zhao, H. Liang, E. Clarke, C. Jackson and M. Xue, Inflammation in Chronic Wounds, *Int. J. Mol. Sci.*, 2016, **17**, 2085.
19 L. A. Wallace, L. Gwynne and T. Jenkins, Challenges and opportunities of pH in chronic wounds, *Ther. Delivery*, 2019, **10**, 719–735.
20 A. Richter, G. Paschew, S. Klatt, J. Lienig, K.-F. Arndt and H.-J. P. Adler, Review on Hydrogel-based pH Sensors and Microsensors, *Sensors*, 2008, **8**, 561–581.
21 C. Rungsima, N. Boonyan, M. Klorvan and B. Kusuktham, Hydrogel sensors with pH sensitivity, *Polym. Bull.*, 2021, **78**, 5769–5787.
22 A. Tamayol, M. Akbari, Y. Zilberman, M. Comotto, E. Lesha, L. Serex, S. Bagherifard, Y. Chen, G. Fu and S. K. Ameri, *et al.*, Flexible pH-Sensing Hydrogel Fibers for Epidermal Applications, *Adv. Healthcare Mater.*, 2016, **5**, 711–719.
23 V. Gounden and M. Singh, Hydrogels and Wound Healing: Current and Future Prospects, *Gels*, 2024, **10**, 43.
24 J. Chalitangkoon and P. Monvisade, Dual pH/thermal-dependent coloring polymeric dye through Mannich reaction of chitosan: Synthesis and characterization, *Carbohydr. Polym.*, 2019, **223**, 115049.
25 M. Lv, Y. Li, X. Qiao, X. Zeng and X. Luo, An antifouling electrochemical biosensor based on oxidized bacterial cellulose and quaternized chitosan for reliable detection of involucrin in wound exudate, *Anal. Chim. Acta*, 2024, **1316**, 342821.
26 D. Lv, J. Cui, Y. Wang, G. Zhu, M. Zhang and X. Li, Synthesis and color properties of novel polymeric dyes based on grafting of anthraquinone derivatives onto O-carboxymethyl chitosan, *RSC Adv.*, 2017, **7**, 33494–33501.

27 L. Tian, A. Singh and A. V. Singh, Synthesis and characterization of pectin-chitosan conjugate for biomedical application, *Int. J. Biol. Macromol.*, 2020, **153**, 533–538.
28 S. Woranuch and R. Yoksan, Preparation, characterization and antioxidant property of water-soluble ferulic acid grafted chitosan, *Carbohydr. Polym.*, 2013, **96**, 495–502.
29 J. Chalitangkoon and P. Monvisade, Synthesis of chitosan-based polymeric dyes as colorimetric pH-sensing materials: Potential for food and biomedical applications, *Carbohydr. Polym.*, 2021, **260**, 117836.
30 E. Schoolaert, I. Steyaert, G. Vancoillie, J. Geltmeyer, K. Lava, R. Hoogenboom and K. D. Clerck, Blend electrospinning of dye-functionalized chitosan and poly(ε-caprolactone): towards biocompatible pH-sensors, *J. Mater. Chem. B*, 2016, **4**, 4507–4516.
31 L. G. Devi, K. S. A. Raju and S. G. Kumar, Photodegradation of methyl red by advanced and homogeneous photo-Fenton's processes: a comparative study and kinetic approach, *J. Environ. Monit.*, 2009, **11**, 1397–1404.
32 L. Ludvíková, P. Friš, D. Heger, P. Šebej, J. Wirz and P. Klán, Photochemistry of rose bengal in water and acetonitrile: a comprehensive kinetic analysis, *Phys. Chem. Chem. Phys.*, 2016, **18**, 16266–16273.
33 V. Trovato, S. Sfameni, G. Rando, G. Rosace, S. Libertino, A. Ferri and M. R. Plutino, A Review of Stimuli-Responsive Smart Materials for Wearable Technology in Healthcare: Retrospective, Perspective, and Prospective, *Molecules*, 2022, **27**, 5709.
34 E. Khadem, M. Kharaziha and S. Salehi, Colorimetric pH-responsive and hemostatic hydrogel-based bioadhesives containing functionalized silver nanoparticles, *Mater. Today Bio*, 2023, **20**, 100650.
35 L. Liu, X. Li, M. Nagao, A. L. Elias, R. Narain and H.-J. Chung, A pH-Indicating Colorimetric Tough Hydrogel Patch towards Applications in a Substrate for Smart Wound Dressings, *Polymers*, 2017, **9**, 558.
36 Y. Zhu, J. Zhang, J. Song, J. Yang, Z. Du, W. Zhao, H. Guo, C. Wen, Q. Li and X. Sui, *et al.*, A Multifunctional Pro-Healing Zwitterionic Hydrogel for Simultaneous Optical Monitoring of pH and Glucose in Diabetic Wound Treatment, *Adv. Funct. Mater.*, 2020, **30**, 1905493.
37 F. Le Guern, V. Mussard, A. Gaucher, M. Rottman and D. Prim, Fluorescein Derivatives as Fluorescent Probes for pH Monitoring along Recent Biological Applications, *Int. J. Mol. Sci.*, 2020, **21**, 9217.
38 M. V. Sednev, C. A. Wurm, V. N. Belov and S. W. Hell, Carborhodol: a new hybrid fluorophore obtained by combination of fluorescein and carbopyronine dye cores, *Bioconjugate Chem.*, 2013, **24**, 690–700.
39 S. Jia, K. M. Ramos-Torres, S. Kolemen, C. M. Ackerman and C. J. Chang, Tuning the Color Palette of Fluorescent Copper Sensors through Systematic Heteroatom Substitution at Rhodol Cores, *ACS Chem. Biol.*, 2018, **13**, 1844–1852.
40 A. Syam, A. Zilles, N. Kemnitzer and J. Arden-Jacob *Dyes with pH-dependent absorption and fluorescence*, EP24200857.1, 2024.
41 J. L. Bachman, C. I. Pavlich, A. J. Boley, E. M. Marcotte and E. V. Anslyn, Synthesis of Carboxy ATTO 647N Using Redox Cycling for Xanthone Access, *Org. Lett.*, 2020, **22**, 381–385.
42 M. M. Sadat Ebrahimi and H. Schönherr, Enzyme-sensing chitosan hydrogels, *Langmuir*, 2014, **30**, 7842–7850.
43 G. Talsky, Spectrometric Titrations. Analysis of Chemical Equilibria. Von J. Polster und H. Lachmann. VCH Verlagsgesellschaft, Weinheim 1989. 433 S., geb. DM 196.00. – ISBN 3-527-26436-1, *Angew. Chem.*, 1990, **102**, 343.
44 G. Giovannini, R. M. Rossi and L. F. Boesel, Changes in Optical Properties upon Dye-Clay Interaction: Experimental Evaluation and Applications, *Nanomaterials*, 2021, **11**, 197.
45 H. Kaczmarek, A. Tafelska-Kaczmarek, K. Roszek, J. Czarnecka, B. Jędrzejewska and K. Zblewska, Fluorescent Chitosan Modified with Heterocyclic Aromatic Dyes, *Materials*, 2021, **14**, 6429.
46 E. Slyusareva, M. Gerasimova, V. Slabko, N. Abuzova, A. Plotnikov and A. Eychmüller, Synthesis and Characterization of Chitosan-Based Polyelectrolyte Complexes Doped with Xanthene Dyes, *ChemPhysChem*, 2015, **16**, 3997–4003.
47 M. Moradi, H. Tajik, H. Almasi, M. Forough and P. Ezati, A novel pH-sensing indicator based on bacterial cellulose nanofibers and black carrot anthocyanins for monitoring fish freshness, *Carbohydr. Polym.*, 2019, **222**, 115030.
48 P. Ezati, H. Tajik and M. Moradi, Fabrication and characterization of alizarin colorimetric indicator based on cellulose-chitosan to monitor the freshness of minced beef, *Sens. Actuators, B*, 2019, **285**, 519–528.
49 L. Prietto, T. C. Mirapalhete, V. Z. Pinto, J. F. Hoffmann, N. L. Vanier, L.-T. Lim, A. R. Guerra Dias and E. Da Rosa Zavareze, pH-sensitive films containing anthocyanins extracted from black bean seed coat and red cabbage, *LWT*, 2017, **80**, 492–500.